

PRECISION MEASUREMENT OF THE MOST DISTANT SPECTROSCOPICALLY CONFIRMED SUPERNOVA Ia WITH THE *HUBBLE SPACE TELESCOPE*¹

D. RUBIN^{2,3}, R. A. KNOP⁴, E. RYKOFF^{2,5}, G. ALDERING², R. AMANULLAH⁶, K. BARBARY², M. S. BURNS⁷, A. CONLEY⁸, N. CONNOLLY⁹, S. DEUSTUA¹⁰, V. FADEYEV¹¹, H. K. FAKHOURI^{2,3}, A. S. FRUCHTER¹⁰, R. A. GIBBONS¹², G. GOLDBABER^{2,3,20}, A. GOOBAR^{6,13}, E. Y. HSIAO^{2,14,15}, X. HUANG³, M. KOWALSKI¹⁶, C. LIDMAN¹⁷, J. MEYERS^{2,3}, J. NORDIN^{2,14}, S. PERLMUTTER^{2,3}, C. SAUNDERS^{2,3}, A. L. SPADAFORA², V. STANISHEV¹⁸, N. SUZUKI^{2,14}, L. WANG¹⁹
(THE SUPERNOVA COSMOLOGY PROJECT)

ApJ Volume 763 Number 1

ABSTRACT

We report the discovery of a redshift 1.71 supernova in the GOODS North field. The *Hubble Space Telescope* (*HST*) ACS spectrum has almost negligible contamination from the host or neighboring galaxies. Although the rest frame sampled range is too blue to include any Si II line, a principal component analysis allows us to confirm it as a Type Ia supernova with 92% confidence. A recent serendipitous archival *HST* WFC3 grism spectrum contributed a key element of the confirmation by giving a host-galaxy redshift of 1.713 ± 0.007 . In addition to being the most distant SN Ia with spectroscopic confirmation, this is the most distant Ia with a precision color measurement. We present the ACS WFC and NICMOS 2 photometry and ACS and WFC3 spectroscopy. Our derived supernova distance is in agreement with the prediction of Λ CDM.

Subject headings: supernovae: general

1. INTRODUCTION

Over the past 15 years, *HST* has played an integral role in measuring cosmological parameters through the Type Ia supernova Hubble diagram (Perlmutter et al. 1998; Garnavich et al. 1998; Riess et al. 1998; Perlmutter et al. 1999; Knop et al.

2003; Riess et al. 2004, 2007; Amanullah et al. 2010; Suzuki et al. 2012). With its low background and diffraction-limited imaging, *HST* is capable of measuring supernovae at redshifts that are very difficult from the ground. Measuring very distant supernovae breaks degeneracies in the lower-redshift Hubble diagram, enabling us to probe the nature of dark energy at redshifts above $z \sim 0.5$ independently of its low-redshift behavior. In this paper, we present the most distant cosmologically useful supernova to date and show that even at this distance, *HST* can still make measurements with precision.

2. SEARCH AND FOLLOWUP

SN SCP-0401 was found in the GOODS North Field (Dickinson et al. 2003) as part of a supernova survey with sets of supernova followup that were alternated between the Supernova Cosmology Project (SCP)²¹ and the Higher-Z SN Search Team²². Four epochs of Advanced Camera for Surveys (ACS) F850LP and F775W (these are z and i -band filters) observations were obtained, with a cadence of ~ 7 weeks. In the first cadenced epoch (2004 April 3), this candidate was discovered in the reference-subtracted²³ F850LP image with a signal-to-noise ratio of 9 (Vega magnitude 25.2, see details of photometry in Section 4). In the concurrent F775W image, it had a signal-to-noise ratio of 2 (Vega 26.5). Because the red observed color implied a possible very-high-redshift SN Ia, we followed it with ACS F850LP and Near Infrared Camera and Multi-Object Spectrometer (NICMOS 2) F110W and F160W (very broad J and H -band filters) photometry, and ACS G800L grism spectroscopy²⁴.

¹ Based on observations with the NASA/ESA *Hubble Space Telescope*, obtained at the Space Telescope Science Institute, which is operated by AURA, Inc., under NASA contract NAS 5-26555, under programs GO-9583, GO-9727, GO-9728, GO-10339, and, GO-11600.

² E.O. Lawrence Berkeley National Lab, 1 Cyclotron Rd., Berkeley, CA, 94720

³ Department of Physics, University of California Berkeley, Berkeley, CA 94720

⁴ Quest University Canada, Squamish, BC, Canada.

⁵ Kavli Institute for Particle Astrophysics and Cosmology, SLAC National Accelerator Laboratory, Menlo Park, CA 94025

⁶ The Oskar Klein Centre, Department of Physics, AlbaNova, Stockholm University, SE-106 91 Stockholm, Sweden

⁷ Colorado College, 14 East Cache La Poudre St., Colorado Springs, CO 80903

⁸ Center for Astrophysics and Space Astronomy, 389 UCB, University of Colorado, Boulder, CO 80309

⁹ Hamilton College Department of Physics, Clinton, NY 13323

¹⁰ Space Telescope Science Institute, 3700 San Martin Drive, Baltimore, MD 21218

¹¹ Santa Cruz Institute for Particle Physics, University of California Santa Cruz, Santa Cruz, CA 94064

¹² Department of Physics and Astronomy, Vanderbilt University, Nashville, TN 37240, USA

¹³ Department of Physics, Stockholm University, Albanova University Center, SE-106 91, Stockholm, Sweden

¹⁴ Space Sciences Lab, 7 Gauss Way, Berkeley, CA 94720

¹⁵ Carnegie Observatories, Las Campanas Observatory, Casilla 601, La Serena, Chile

¹⁶ Physikalisches Institut Universität Bonn, Germany

¹⁷ Australian Astronomical Observatory, PO Box 296, Epping, NSW 1710, Australia

¹⁸ CENTRA - Centro Multidisciplinar de Astrofísica, Instituto Superior Técnico, Av. Rovisco Pais 1, 1049-001 Lisbon, Portugal

¹⁹ Department of Physics, Texas A & M University, College Station, TX 77843, USA

²⁰ Deceased

²¹ HST GO Program 9727

²² HST GO Program 9728

²³ The reference images for this field come from Program ID 9583.

²⁴ This supernova is referred to in the HST archive as SN150G and elsewhere by its nickname “Mingus” (Gibbons et al. 2004).

The sky in the vicinity of the SN is shown in Figure 1²⁵. The likely host is the late-type galaxy at redshift 1.713 (see Section 3.2) centered 0.8'' away. This corresponds to only 7 kpc if the SN and galaxy are at the same distance. Light from this galaxy is visible at the location of the supernova and no other galaxies down to a magnitude limit of AB \sim 26.5 F775W are within 3.5''. In the F775W and redder data, this galaxy has two cores, indicating a possible merger. The consistency of the colors of these cores (always < 0.3 mag, typically < 0.1) over the wide range of 4350Å to 16000Å makes it extremely likely that these cores are at the same redshift.

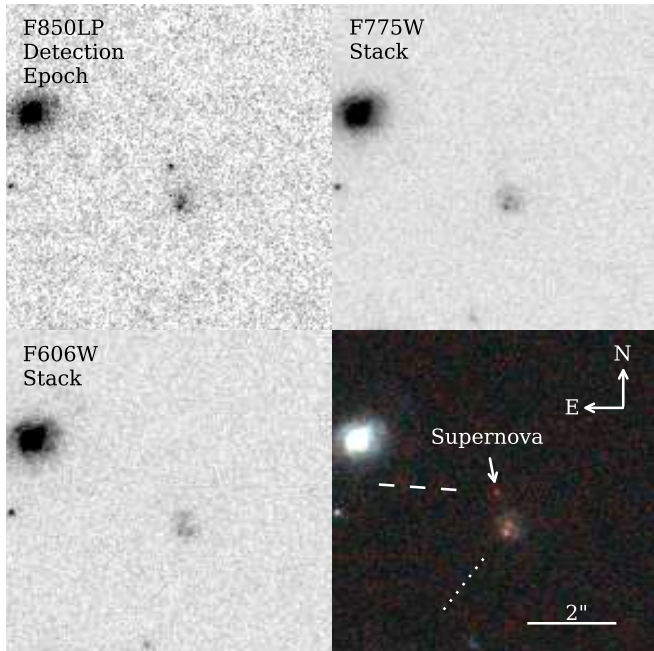


FIG. 1.— ACS images of the supernova location. The lower right panel shows a three-component color image composed from: an F606W stack (blue), F775W stack (green), and the F850LP SN detection epoch (red), which are shown in the remaining panels. The lines indicate the dispersion direction in ACS (dashed) and WFC3 (dotted) spectroscopy. The supernova coordinates are 12:37:09.5 +62:22:15.5 (J2000.0).

3. SPECTROSCOPY

3.1. ACS Grism Observations of SN and Host

We obtained eleven orbits of spectroscopy with the ACS G800L grism nine days after the discovery epoch. The light curve fit (Section 5.1) indicates that the spectrum was taken 2 ± 3 rest-frame days after rest-frame *B*-maximum. We extracted spectra for the likely host and SN with aXe (Kümmel et al. 2009). No conclusive features or lines were apparent in the spectrum of the galaxy, nor did the two cores give significantly different spectra.

3.2. Wide Field Camera 3 Grism Observations of the Host

²⁵ In addition to the other datasets, data from HST GO Program 10339 was used for this figure and the subsequent host-galaxy analysis.

As a fortunate coincidence, two orbits of Wide Field Camera 3 (WFC3) IR G141 grism spectroscopy were taken in this region of GOODS North on 2010-09-26²⁶. Although the F140W direct image missed the host galaxy, the grism dispersed the host into the field of view. Matching objects between ACS F850LP imaging and the direct image allowed us to compute the position of the host galaxy for use by aXe.

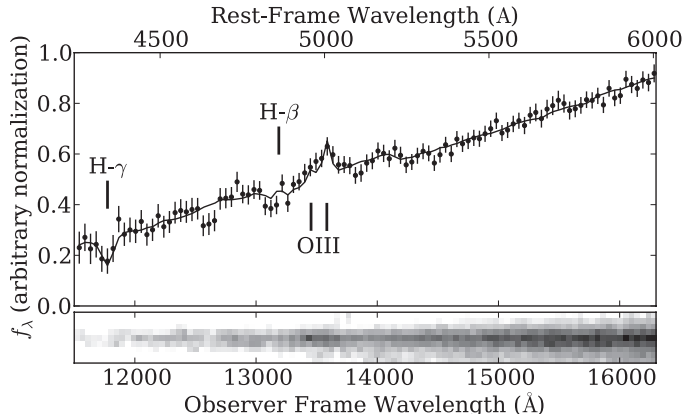


FIG. 2.— Upper panel: Extracted WFC3 IR spectrum of the likely host galaxy with template fit using SDSS galaxy principal components (solid line). The best-fit (and only reasonable) redshift is 1.713. We note that including the ACS grism data for the host (5500Å to 10000Å) has no effect on the fit. Lower panel: 2D WFC3 spectrum, spanning 103 pixels. Some of the flux visible at longer wavelengths than the features is contamination.

The host galaxy spectrum is shown in Figure 2, along with the best-fit template derived by scaling principal components of SDSS spectra (Aihara et al. 2011). Only one feature is detected at very high statistical significance: an emission feature at 13600Å. The only reasonable match to the spectrum between redshift 1.0 and 2.0 is one centered on redshift 1.713. The emission feature is then made up of a blend of the [OIII] $\lambda\lambda$ 4959, 5007Å doublet. No other emission lines are required to appear in the wavelength range of either grism spectrum for this to be a credible template match. We also see possible absorption from H γ and H β (4340Å, and 4861Å rest-frame wavelengths, respectively), but at lower statistical significance. As we are not sure which core (or both) emit the [OIII], we take a conservative 0.1'' separation = 36Å systematic uncertainty in the observer-frame wavelength of the lines. This translates to a 0.007 uncertainty on the redshift, which dominates the other sources of uncertainty.

3.3. Typing

aXe resamples the grism data, correlating neighboring flux measurements. This can be seen by eye in the spectrum (points with errorbars in Figure 3), that is, the difference between neighboring flux measurements is generally smaller than one would expect from the indicated error bars. These positive correlations reduce the statistical significance of spectral features, so a quantitative understanding of these correlations is crucial. By examining blank sky, we find that the correlation between

²⁶ Data from HST GO Program 11600

neighboring errors is 0.4 (and confirm the accuracy of the on-diagonal errors reported by aXe). The weight of the spectrum scales with the correlation between neighbors (ρ) as $1/(1 + 2\rho)$ (see Appendix A for the derivation). The weight of the spectrum is thus reduced by 44% compared to a naive reading of the aXe error bars. All χ^2 values in this paper are computed using a covariance matrix containing nearest-neighbor correlations.

As our supernova spectrum misses the Si II $\lambda 6355$ (Wheeler & Levreault 1985; Uomoto & Kirshner 1985; Panagia 1985) and Si II $\lambda 4130$ (Clocchiatti et al. 2000) lines normally used for confirming SNe Ia, we use statistical methods for classifying SN SCP-0401.

We first begin by collecting the comparison rest-frame UV spectra available to us. A useful list of SNe observed with the *HST* and the *International Ultraviolet Explorer* (*IUE*) is Panagia (2003), with an updated list, including *Swift*-observed, in Brown (2009). We obtained *IUE* spectra and *HST* spectra from the Mikulski Archive for Space Telescopes (MAST)²⁷, and *Swift* spectra from the SUSPECT archive²⁸. More recent spectra were found by searching MAST, others came from the literature. A summary of all data is given in Table 1; we collect 94 spectra in total from 33 SNe, all within ~ 2 weeks of B or V -maximum (whichever is quoted in the literature).

Our goal is to compare these spectra to the spectrum of SN SCP-0401, extracting a probability of matching for each. Unfortunately, most of the data are from the *IUE*, and only extend to $\sim 3300\text{\AA}$ observer-frame, rather than 3600\AA as we have with SN SCP-0401 (a related issue is the presence of noise in the comparison spectra). This limitation complicates the comparison of these spectra to SN SCP-0401.

Another, more subtle, issue is also relevant. We note that simply converting a χ^2 per degree of freedom to a probability (e.g., Rodney et al. 2012) is never appropriate when comparing different models to the same data. $\Delta\chi^2$ values (the difference in χ^2 between models) can be converted into probabilities, but this requires knowing the dimensionality of the parameter space²⁹.

We can address both issues (limited coverage and estimating dimensionality) by performing a principal component analysis of all spectra in the UV. The details are discussed in Appendix B. After computing the mean and first two principal components, we can compute a $\Delta\chi^2$ between SN SCP-0401 and every other spectrum in turn. We fit SN SCP-0401 and another spectrum with the projections onto the components constrained to be the same (we allow them to have different normalizations); this gives us a joint χ^2 . We then subtract the χ^2 values for SN SCP-0401 and the other spectrum when they are allowed to have different projections. This $\Delta\chi^2$ value gives us the probability that the SNe have different true projections given the observed data. We then subtract this value from 1 to get a “matching probability.”

These results are summarized in Table 2. Thirteen SNe have matching probabilities above 0.05; twelve of

these (and all of the top six) are SNe Ia. The average matching probability of a SN Ia is 41.8%; the average probability for a core-collapse SN is 3.4%. The probability of SN SCP-0401 being a Ia from the spectrum alone (assuming an equal fraction of SNe Ia and CC SNe; see below) is therefore $41.8/(3.4 + 41.8) = 92\%$. In Figure 3, we plot the best-matching spectrum of the five best-matching SNe of each type. Of the CC SNe, only SN1983N is a credible match spectroscopically, although this supernova was two magnitudes fainter at maximum than a typical SN Ia (Prabhu 1985).

We now must evaluate the relative ratio of CC SNe to SNe Ia at redshift 1.713 for SNe with comparable brightness to SNe Ia. Bazin et al. (2009) present both photometrically and spectroscopically classified SNe from the Supernova Legacy Survey and the associated absolute magnitudes (their definition is similar to a V -band AB absolute magnitude). For SNe with brightness comparable to most SNe Ia (~ -19), they find a SN Ia to CC rate of ~ 5 -to-1 at redshift 0.3. However, at redshift 1.713, the star-formation rate is ~ 5 times higher than at redshift 0.3 (Hopkins & Beacom 2006), raising the core-collapse rate by approximately the same value. The SN Ia rate is equal to within the error bars (tens of percent) at redshift 0.3 and redshift 1.713 (Barbary et al. 2012), so both classes of SNe are comparably common at this redshift. We therefore retain the 92% confidence that was derived ignoring the rates.

It is also encouraging that the spectrum of SN SCP-0401 matches the theoretical SN Ia spectra of Lentz et al. (2000) derived from the W7 model (Nomoto et al. 1984) (see Table 2). The best match is for the unscaled heavy element abundance (that is, no change from W7).

As a less-likely possibility, we investigate the possibility that the nearby galaxy is not the host. We use the spectra with broad wavelength coverage (almost all of those in Table 1 except the *IUE* spectra) and match them against SN SCP-0401 with the redshift floating. It is reassuring that the best match is a Ia (SN1992A) at redshift 1.72, at least for this limited set of SNe.

This analysis may turn out to be conservative. In the Lick Observatory Supernova Search volume-limited sample (Li et al. 2011), the ratio of SNe II to SNe Ibc is about 3-to-1, similar to what we have in our sample of spectra. However, the SNe Ibc are fainter on average than SNe II; in Bazin et al. (2009), the ratio appears to be higher (in the luminosity range of SNe Ia). If SNe Ibc are the only plausible non-Ia match to SN SCP-0401, then our confidence that SN SCP-0401 is a SN Ia may get stronger simply from revised rates. It is also possible that no SNe Ibc are credible matches to SN SCP-0401, and more wavelength coverage of SN1983N would have shown us that it does not match. In the future, additional core-collapse comparison spectra will resolve this question.

4. SN PHOTOMETRY

We used similar techniques for the SN photometry as were used in Suzuki et al. (2012); these are summarized below. In the spirit of “blinded” analysis, we finalize the photometry before looking at the light curve or distance modulus. We give our photometry in Table 3.

4.1. ACS Photometry

²⁷ <http://archive.stsci.edu/>

²⁸ <http://suspect.nhn.ou.edu>

²⁹ A well-known example is the 68.3% confidence interval, which is given (in the assumption of Gaussian errors and an approximately linear model) by $\Delta\chi^2 < 1$ in one dimension and $\Delta\chi^2 < 2.30$ in two.

TABLE 1
COMPARISON SPECTRUM SOURCES

SN	Type	Type Reference	Phase	Date of Maximum Reference	Source and Program ID
1978G	II	Ward et al. (1978)	Discovery +5, +16	Ward et al. (1978)	<i>IUE</i> OD7AB
1979C	II	Mattei et al. (1979)	+6 to +16	de Vaucouleurs et al. (1981)	<i>IUE</i> CVBCW, ESATO, UKTOO, CVBCW
1980K	II	Kirshner & Bryan (1980)	~ 0	Buta (1982)	<i>IUE</i> VILSP, CVBCW, UKTOO
1980N	Ia	Blanco et al. (1980)	-1 to +12	Hamuy et al. (1991a)	<i>IUE</i> CVBCW, VILSP
1981B	Ia	Vettolani et al. (1981)	+2, +3	Branch et al. (1983)	<i>IUE</i> VILSP, NP314
1982B	Ia	Szeidl et al. (1982)	+2	Ciatti et al. (1988)	<i>IUE</i> NP586
1983G	Ia	Wamsteker et al. (1983)	+3, +6, +9	Buta et al. (1985)	<i>IUE</i> SNFRK, FE022
1983N	Ib	Prabhu (1985)	-13 to +13	N. Panagia, in Branch et al. (2002)	<i>IUE</i> FE022, FETOO, SNFRK, OD15K
1985L	II	Filippenko et al. (1985)	+12	Kimeridze & Tsvetkov (1989)	<i>IUE</i> HQTOO
1987A	II	Herald et al. (1987)	-16, 0, +14	Gouiffes et al. (1988)	<i>IUE</i> OD17Y
1989B	Ia	Korth (1989)	-9, -10	Prabhu & Krishnamurthi (1990)	<i>IUE</i> STKRK
1989M	Ia	Kharadze et al. (1989)	0 to +13	Kimeridze & Tsvetkov (1991)	<i>IUE</i> LETOO, SNLRK, LE059
1990M	Ia	Sonneborn et al. (1990)	-6, -3	Polcaro & Viotti (1991)	<i>IUE</i> SNMRK
1990N	Ia	Maury et al. (1990)	-10 to +4	Leibundgut et al. (1991)	<i>IUE</i> SNMRK
1990W	Ic	della Valle et al. (1990)	+4	della Valle et al. (1990)	<i>IUE</i> SNMRK
1991T	Ia	Hamuy et al. (1991b)	+8, +10	Phillips et al. (1992)	<i>IUE</i> METOO, SNMRK
1992A	Ia	Liller et al. (1992)	-2 to +11	Suntzeff et al. (1992)	<i>IUE</i> SNNRK and <i>HST</i> FOS 4016
1993J	Ib	Prabhu (1995)	-11, -3	Prabhu (1995)	<i>IUE</i> SNORK and <i>HST</i> FOS 4528
1994I	Ic	Filippenko et al. (1994)	+10	Richmond, in Sasaki et al. (1994)	<i>HST</i> FOS 5623
1997ap	Ia	Perlmutter et al. (1998)	-2	Perlmutter et al. (1998)	Keck II, Perlmutter et al. (1998)
1998S	II	Li et al. (1998)	+4	Liu et al. (2000)	<i>HST</i> STIS 7434
1999em	II	Jha et al. (1999)	+5	Hamuy et al. (2001)	<i>HST</i> STIS 8243
2001eh	Ia	Ganeshalingam et al. (2001)	+7	SALT2-2 fit to Hicken et al. (2009)	<i>HST</i> STIS 9114
2001ep	Ia	Matheson et al. (2001)	+9, +15	SALT2-2 fit to Hicken et al. (2009)	<i>HST</i> STIS 9114
2001ig	Ib	Phillips et al. (2001)	Discovery +4, +12	Evans et al. (2001)	<i>HST</i> STIS 9114
2002ap	Ic	Kawabata et al. (2002)	-5	Foley et al. (2003)	<i>HST</i> STIS 9114
2005cf	Ia	Modjaz et al. (2005a)	-9 to +4	SALT2-2 fit to Hicken et al. (2009)	<i>Swift</i> UVOT, Bufano et al. (2009)
2005cs	II	Modjaz et al. (2005b)	+9, +11	Pastorello et al. (2009)	<i>Swift</i> UVOT, Bufano et al. (2009)
2006jc	Ib	Immler (2005)	0	Foley et al. (2007)	<i>Swift</i> UVOT, Bufano et al. (2009)
2010al	II	Kirshner et al. (2010)	< 0	Kirshner et al. (2010)	<i>HST</i> STIS 11654
2011dh	Ib	Stringfellow et al. (2011)	+6	Tsvetkov et al. (2012)	<i>HST</i> STIS 12540
2011iv	Ia	Drescher et al. (2011)	+1	Foley et al. (2012)	<i>HST</i> STIS 12592, Foley et al. (2012)
SNLS	Ia	Ellis et al. (2008)	0	Ellis et al. (2008)	Ellis et al. (2008)
Ia Model	Ia	Lentz et al. (2000)	0 (Explosion +20)	Lentz et al. (2000)	Lentz et al. (2000)

NOTE. — Sources of data for the principal component analysis, indicating the SN type, source, and phase (phase range for many collected spectra from the same SN). *IUE* is the *International Ultraviolet Explorer*, *HST* FOS/ STIS are the *Hubble Space Telescope* Faint Object Spectrograph and Space Telescope Imaging Spectrograph, and *Swift* UVOT is the *Swift* Ultraviolet/Optical Telescope. The *IUE* spectra extend blueward of ~ 3300Å rest frame, the *HST*, *Swift*, and Lentz spectra cover the whole wavelength range, the spectrum of 1997ap covers redward of ~ 2700Å rest frame, and the Ellis composite covers redward of ~ 2800Å rest frame.

TABLE 2
PROBABILITIES OF MATCHING SN SCP-0401.

Supernova	Type	Probability of Match
SN1980N	Ia	0.969
SN2001ep	Ia	0.968
SN1981B	Ia	0.963
SN1992A	Ia	0.924
SN2011iv	Ia	0.886
SN1990N	Ia	0.610
Lentz et al. (2000)	Ia Model	0.514
SN1983N	Ib	0.489
SN2001eh	Ia	0.420
SN1989M	Ia	0.316
SN1982B	Ia	0.244
SN1990M	Ia	0.157
SN1989B	Ia	0.139
SN1991T	Ia	0.059

NOTE. — Probabilities of each supernova matching SN SCP-0401. The values are taken from the principal-component-like analysis described in Section 3.3 and Appendix B. Only probabilities greater than 0.05 are shown.

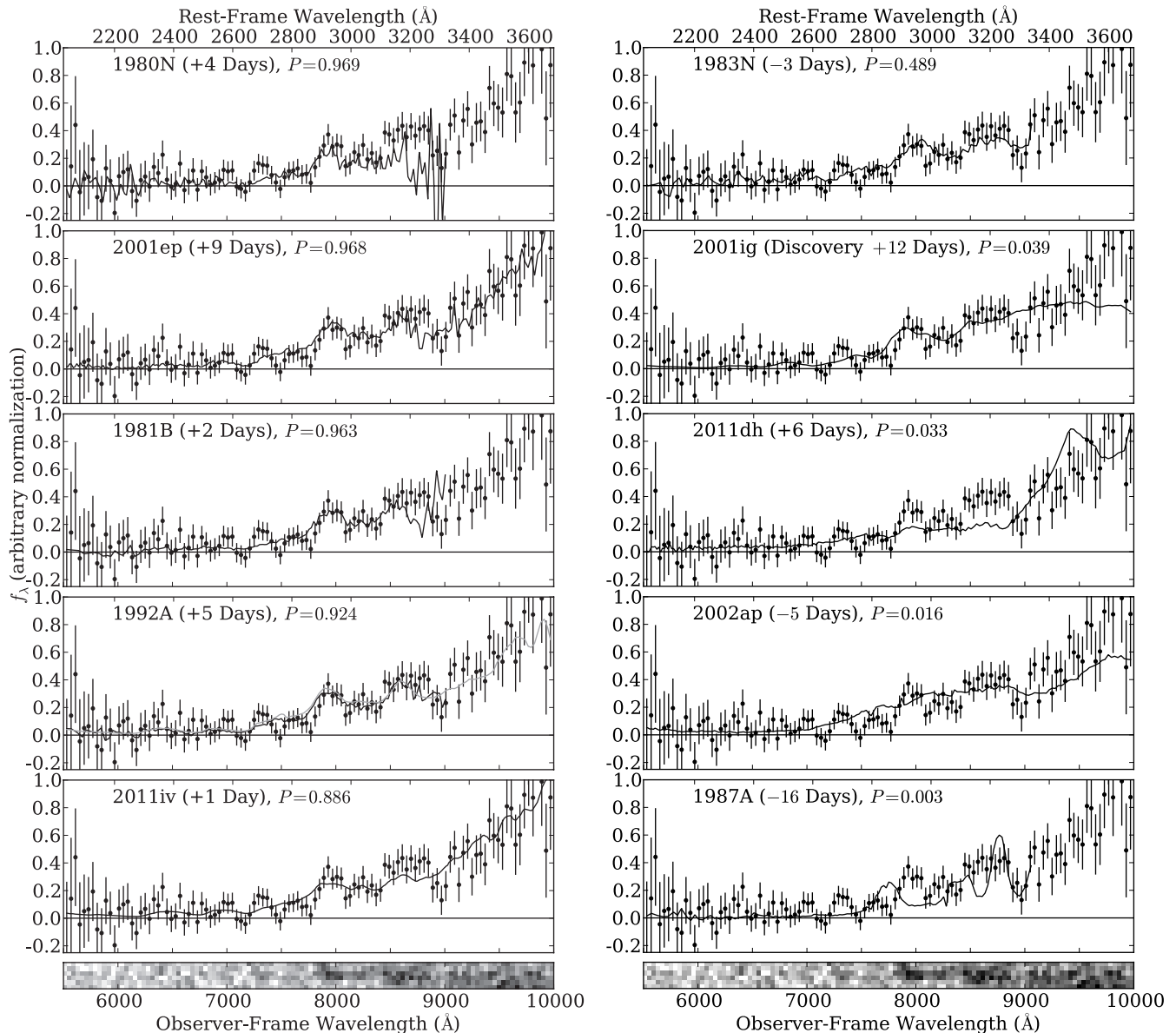


FIG. 3.— Each panel shows a comparison between SN SCP-0401 (points with error bars) and another SN. The five best-matching comparison SNe Ia are shown in the left panels; the five best-matching comparison CC SNe are shown in the right panels. For each comparison SN, only the best-matching epoch is shown. The best visual match is SN1992A (left, third from top); we have overlaid additional data from a phase of +8 days that covers the full rest-frame wavelength range (light grey), showing that the match continues for the full spectrum. Of the 17 CC SNe (the best five of which are shown here), only SN1983N is a possible match, although as noted in the text, this SN is two magnitudes fainter at max than a typical SN Ia. Bottom panels: 2D SN SCP-0401 spectrum, spanning 112 pixels. Some of the flux visible in the very reddest wavelengths is contamination from a nearby galaxy.

TABLE 3
PHOTOMETRY OF SN SCP-0401.

MJD	PID	Camera	Filter	Exposure (s)	Flux (DN/s)	Flux Error (DN/s)	Vega=0 Zeropoint
52600.72	9583	ACS WFC	F775W	1120.0	-0.0426	0.0599	25.291
52600.75	9583	ACS WFC	F850LP	2400.0	-0.0206	0.0274	23.909
52643.38	9583	ACS WFC	F775W	1000.0	-0.0271	0.0669	25.291
52643.43	9583	ACS WFC	F850LP	2120.0	0.0180	0.0293	23.909
52691.46	9583	ACS WFC	F775W	960.0	-0.0422	0.0655	25.291
52691.52	9583	ACS WFC	F850LP	2060.0	0.0014	0.0288	23.909
52734.16	9583	ACS WFC	F775W	960.0	0.1358	0.0599	25.291
52734.22	9583	ACS WFC	F850LP	2000.0	-0.0128	0.0255	23.909
52782.70	9583	ACS WFC	F775W	960.0	0.0864	0.0573	25.291
52782.78	9583	ACS WFC	F850LP	2080.0	-0.0048	0.0259	23.909
53098.41	9727	ACS WFC	F850LP	1600.0	0.3249	0.0371	23.909
53098.43	9727	ACS WFC	F775W	400.0	0.3328	0.1369	25.291
53107.15	9727	ACS WFC	F850LP	4564.0	0.2213	0.0237	23.909
53111.21	9727	NICMOS 2	F110W	2687.9	0.2427	0.0144	23.029
53111.31	9727	NICMOS 2	F160W	5375.7	0.2011	0.0125	22.160
53121.57	9727	ACS WFC	F850LP	4384.0	0.1311	0.0210	23.909
53130.83	9727	NICMOS 2	F160W	5375.7	0.1387	0.0120	22.160
53136.86	9727	NICMOS 2	F110W	2687.9	0.1205	0.0154	23.029
53142.59	9727	NICMOS 2	F160W	8063.6	0.1158	0.0103	22.160
53145.98	9728	ACS WFC	F775W	400.0	-0.0623	0.1536	25.291
53146.01	9728	ACS WFC	F850LP	1600.0	-0.0287	0.0361	23.909
53148.41	9727	NICMOS 2	F110W	8063.6	0.0811	0.0113	23.029
53196.34	9727	ACS WFC	F850LP	1600.0	0.0536	0.0392	23.909
53196.37	9727	ACS WFC	F775W	400.0	0.1695	0.1701	25.291
53244.51	9728	ACS WFC	F775W	400.0	-0.1195	0.1573	25.291
53244.54	9728	ACS WFC	F850LP	1600.0	0.0003	0.0345	23.909
53284.82	10339	ACS WFC	F775W	375.0	-0.1097	0.1749	25.291
53284.84	10339	ACS WFC	F850LP	1400.0	-0.0009	0.0580	23.909
53333.94	10339	ACS WFC	F775W	400.0	-0.1821	0.1886	25.291
53333.98	10339	ACS WFC	F850LP	1540.0	-0.0756	0.0471	23.909
53377.72	10339	ACS WFC	F775W	355.0	-0.2258	0.2653	25.291
53377.74	10339	ACS WFC	F850LP	1520.0	-0.0214	0.0488	23.909
53427.73	10339	ACS WFC	F775W	375.0	0.0921	0.2744	25.291
53427.76	10339	ACS WFC	F850LP	1540.0	0.0346	0.0429	23.909
53473.53	10339	ACS WFC	F775W	425.0	-0.0096	0.1364	25.291
53473.55	10339	ACS WFC	F850LP	1700.0	0.0359	0.0331	23.909

NOTE. — Due to the uncertainty on the galaxy models, the NICMOS F110W statistical errors share an off-diagonal covariance of $3.46\text{e-}5 \text{ DN/s}^2$, while the F160W errors share a separate off-diagonal covariance of $1.97\text{e-}5 \text{ DN/s}^2$. The ACS statistical errors are diagonal.

We begin by iteratively combining each epoch with MultiDrizzle (Fruchter & Hook 2002; Koekemoer et al. 2002) and aligning all epochs. Aperture photometry with a three-pixel radius ($0.15''$) is computed for all epochs, with the zero level set by the many epochs without the SN. As the pixel values in the resampled images are correlated, the background error is derived empirically (by placing many three-pixel radius apertures in object-free parts of the image), and the Poisson error of the aperture flux is added in quadrature. We use a zeropoint of 23.909 (Vega = 0) for the F850LP data, derived in Suzuki et al. (2012) along with the effective throughput, and 25.291 (Vega = 0) for the F775W data, from Bohlin (2007).

4.2. NICMOS Photometry

The optimal radius for aperture photometry with NICMOS is approximately 1 pixel ($0.076''$), precluding any resampling of the NICMOS images. Following Suzuki et al. (2012), we therefore performed the NICMOS photometry using analytic galaxy models (one for each filter) which were convolved with their PSFs and resampled to match the images. The supernova position and fluxes were modeled simultaneously using PSFs generated for each spectral energy distribution (SED) and band. As there are two cores for this galaxy, we use two azimuthally symmetric elliptical models (with radial variation described by splines) to model the cores (as the SN is reasonably far off-core, this is mainly needed to get the centroid of the model correct for each image). The remaining azimuthal asymmetry of the galaxy was modeled with a two-dimensional second-order spline, with nodes spaced every five pixels ($0.38''$).

While optimizing the host-galaxy model (e.g., the spline-node spacing), we use simulated SNe at dozens of positions at comparable separation from the galaxy to check for any bias or unexplained variance in the photometry. No bias is seen at the 0.01 magnitude level in either band. However, the final epoch in F110W shows a small amount of unexplained variance (χ^2/degree of freedom 1.35) for the recovered fluxes around the true flux, possibly due to slight South Atlantic Anomaly persistence. We rescale the photometry error bar for this epoch to make the χ^2 per degree of freedom 1.

We used a NICMOS F110W zeropoint of 23.757 AB (23.029 Vega = 0) (Ripoche et al. ApJ Submitted) and a NICMOS F160W zeropoint of 22.16 (Vega = 0) (see discussion in Amanullah et al. 2010).

5. ANALYSIS

5.1. Light-Curve Fit

We fit the light curve of the SN with SALT2-2 (Guy et al. 2010), a principal component expansion of type Ia supernova SEDs. The fit parameters are the date of rest-frame B -band maximum, the magnitude at maximum (m_B), the broadband color (c , similar to a rest-frame $B - V$ color), and light-curve width (x_1 , the next supernova principal component after color). We find $m_B, x_1, c = (26.14, 0.2, -0.10)$. The best-fit template is shown in Figure 4. The corrected-distance-modulus statistical error is only 0.15 mag. (This value does not include Hubble diagram dispersion that cannot be removed with the magnitude corrections detailed in Section 6.) As we lack a measurement on the rise of SN SCP-0401, the

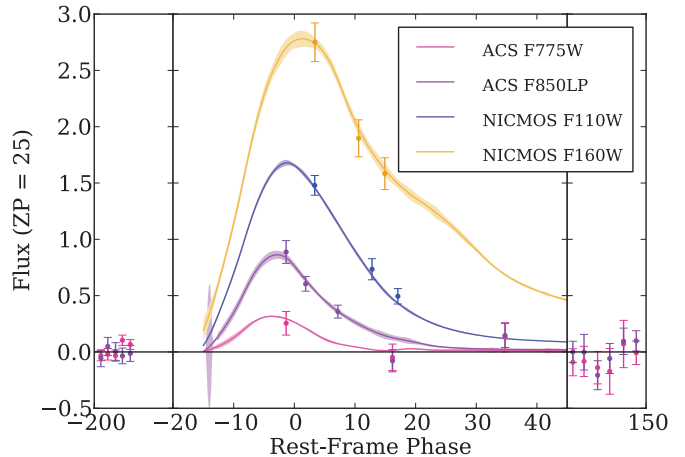


FIG. 4.— SALT2-2 fit to the photometry. To illustrate the quality of the F775W data, the F775W photometry is shown in this plot; as it is too blue for SALT2-2 to fit reliably, these data are not used in any analysis. The error snakes represent the model errors of SALT2-2.

date-of-maximum constraints are asymmetric. We derive the distance modulus uncertainty by sampling from the true corrected distance modulus distribution (by running a Metropolis-Hastings Monte Carlo using the SALT2-2 model). There is a fortuitous cancellation between the date of maximum and the light curve parameters: moving the date of maximum earlier brightens the peak magnitude while increasing the light-curve width and making the color slightly bluer. After applying the corrections in Section 6, the corrected-magnitude likelihood is well-constrained (and is Gaussian).

5.2. Host Stellar Mass

As SALT2 Hubble residuals are correlated with host-galaxy stellar mass (Kelly et al. 2010; Sullivan et al. 2010), we must estimate the host mass for SN SCP-0401. We used a Z-PEG (Le Borgne & Rocca-Volmerange 2002) fit to broad-band galaxy photometry, similar to the methods used in those papers. Using aperture photometry with a $1''$ radius, and zeropoints from Bohlin (2007), we derived the following AB magnitudes for the host galaxy: 25.7 (F435W), 25.2 (F606W), 24.2 (F775W), 23.4 (F850LP), and 20.0 (F160W, Vega = 0). To accurately fit all photometry, Z-PEG requires a template with age 5 Gyr, which is older than the universe at this redshift (4 Gyr). The stellar mass confidence interval when enforcing an age-of-the-universe constraint is essentially contained inside the confidence interval when allowing age to be unconstrained. To be conservative, we do not enforce this constraint, obtaining a \log_{10} stellar mass of $11.2^{+0.1}_{-0.4}$, easily putting this galaxy inside the high-mass ($> 10^{10} M_{\odot}$) category.

5.3. Systematic Errors

5.3.1. Calibration

Fitting an accurate corrected magnitude requires fitting an accurate color (c). The farther apart the filters used are in wavelength, the less (uncorrelated) calibration uncertainties affect the derived c , and therefore the derived corrected magnitude. For a given range of wavelength coverage, measuring a supernova in more filters

will also decrease the sensitivity of the fit to any given miscalibration (again assuming independent calibration uncertainties for the data in each filter). With three passbands within the SALT2-2 range and a long wavelength baseline, the SN distance modulus we derive from the light curve fit is more resilient against calibration uncertainties than most high-redshift SNe distances. Our distance modulus is most sensitive to the F160W zeropoint, with $\partial\mu/\partial(\text{F160W zeropoint}) = 1.5$ (that is, a change in the F160W zeropoint of 0.01 magnitudes changes the corrected magnitude by 0.15), a factor of two better than is typically achieved with only one color. The other calibration uncertainties combine to a systematic error of only ~ 0.01 mag on the distance modulus.

The NICMOS 2 F160W data are affected by a count-rate nonlinearity of 0.026 ± 0.015 mag/dex (de Jong et al. 2006), which adds an effective zeropoint uncertainty of 0.06 magnitudes at the flux level of high-redshift SNe, assuming a power-law dependence of the non-linearity over the full range of flux between the standard stars and the SNe (4-5 dex). Based on the F110W results of Ripoche et al. (ApJ Submitted), we add an uncertainty of 0.03 magnitudes to account for possible deviation from a power law. We will improve this uncertainty with a future recalibration of the F160W non-linearity using the techniques in Ripoche et al. in a future paper.

5.3.2. Malmquist Bias

Most SNe Ia at redshift 1.71 would be too faint to be found by the search, even at maximum brightness. Malmquist bias is therefore present. Most of this bias is taken out by making the corrections we describe in Section 6, but some bias remains. (If it were possible to perfectly correct SNe, such that all SNe were equally bright after correction, no Malmquist bias would remain.) A simple simulation (detailed further in Rubin et al., in prep) that selects SNe from the parent distribution and determines if they could be found at redshift 1.71 allows us to estimate that this remaining Malmquist bias is about 0.08 mag.

If there are SNe at high enough significance to find, but not to get a spectrum of, there may be additional Malmquist bias. We investigate this possibility here using the observed spectrum of SN SCP-0401. The faintest supernova we could have found would be $S/N \sim 5$, rather than $S/N \sim 9$. Increasing the noise in the spectrum by a factor 1.8 allows more supernovae of both types to match the spectrum. The net effect is to lower the confidence of being a Ia to 86%, in which case we would still use the supernova for cosmological analysis. (In an earlier study (Kowalski et al. 2008), we showed that the analysis is robust to this level of non Ia contamination.)

The largest contributors to the Malmquist bias uncertainty are the magnitude cut for the search (which we take to be uncertain at the 0.2 mag level) and the uncorrected residual dispersion of SNe at redshift 1.71 (which we take to be 0.20 ± 0.05 (see discussions below in Sections 5.3.3 and 6)). Each of these contributes about 0.03 magnitudes to the Malmquist bias uncertainty. Therefore, the total uncertainty, which would correlate from supernova-to-supernova were there others like it, is about 0.04 mag.

5.3.3. Lensing

The bright spiral galaxy $3.5''$ away from the supernova (visible to its upper left in Figure 1) is at redshift 0.64 (Cowie et al. 2004), and is thus a potential source of gravitational magnification for the supernova. Here, we provide a rough estimate of the size of this effect.

As with the host galaxy, we used Z-PEG to derive the stellar mass. For this larger (apparent size) galaxy, we used a $1.5''$ radius, and obtained the following AB magnitudes: 23.5 (F435W), 22.7 (F606W), 21.8 (F775W), and 21.5 (F850LP). We use the Z-PEG stellar mass of $4 \times 10^{10} M_{\odot}$ with the relation between stellar mass and halo mass from Guo et al. (2010) to derive the total mass of the halo, $1.4 \times 10^{12} M_{\odot}$. Assuming a singular isothermal sphere model, with $M_{200} \sim M_{\text{halo}}$, we find a magnification of 1.08 (using the Navarro et al. (1996) NFW profile provides virtually the same answer). This number is not the magnification of the supernova; had the lensing galaxy not been there, the supernova would likely be slightly de-magnified (compared to a filled-beam distance modulus). Holz & Linder (2005) find that the scatter due to lensing is approximately $0.093z = 0.16$ magnitudes at this redshift. We include this uncertainty in our distance modulus error (as noted below) and see no evidence that SN SCP-0401 is magnified or de-magnified by more than this.

The mean magnification of supernova fluxes is zero at a given redshift. (Selection effects can bias the observed SNe to higher magnification, but Jönsson et al. (2006) see no evidence of this in the Riess et al. (2004) sample.) However, we fit our cosmological constraints in $\log(\text{flux})$ (magnitudes), where the mean magnification is not zero (as supernova fluxes are roughly log-normally distributed, and we use least-squares fitting, fitting in magnitudes is appropriate). We evaluate the lensing bias from working with magnitudes using the distributions of Wang et al. (2002) and find it to be 0.01 mag (biased faint). In principle, most of this bias is well-understood (from knowledge of the corrected supernova luminosity distribution and the lensing distribution) and could be removed.

6. CONCLUSIONS

We apply the corrections detailed in Suzuki et al. (2012) Equation 3 to obtain a SALT2-2 distance modulus corrected for x_1 , c , and host mass, reproduced here.

$$\mu_B = m_B + \alpha \cdot x_1 - \beta \cdot c + \delta \cdot P(m_{\star}^{\text{true}} < 10^{10} M_{\odot}) - M_B, \quad (1)$$

where α is the light-curve-width-correction coefficient, β is the color-correction coefficient, δ is the host-mass-correction coefficient, and M_B is the ($h = 0.70$) absolute B -magnitude. In addition to the propagated lightcurve fit uncertainties, we add in quadrature the distance modulus scatter due to lensing (above) and σ_{sample} , the error needed to get a χ^2 per degree of freedom of 1 around the Hubble line for the GOODS SNe. We take $M_B = -19.09$, $\alpha = 0.14$, $\beta = 3.1$, $\delta = -0.07$, $\sigma_{\text{sample}} = 0.11$ (Rubin et al., in prep) and find a distance modulus (no magnification or Malmquist bias correction) of 45.57 ± 0.24 statistical, $\pm \sim 0.1$ systematic. This is fully consistent with the value of 45.60 predicted from a flat $\Omega_m = 0.27$ Λ CDM universe. Figure 5 shows the Hubble diagram of Suzuki et al. (2012) with SN SCP-0401 and Primo (Rodney et al. 2012) added. As SALT was updated from

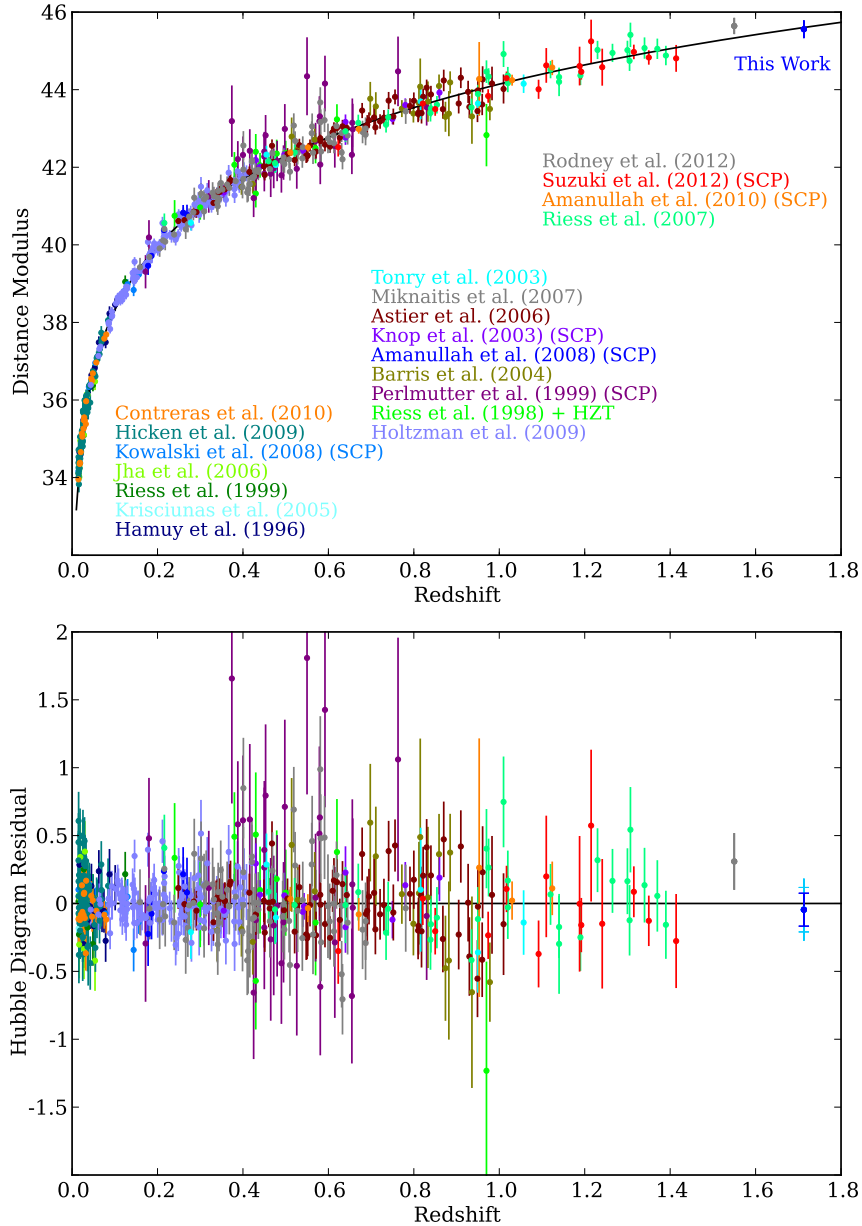


FIG. 5.— Top Panel: Suzuki et al. (2012) Hubble diagram (with the best-fit flat Λ CDM model) with Primo (Rodney et al. 2012) and SN SCP-0401 added.

Bottom Panel: Hubble diagram residuals. The inner (blue) error bars on SN SCP-0401 show the uncertainty of the light-curve fit. The middle (capped, cyan) error bars include the sample dispersion; the outer error bars include the lensing dispersion. Future analyses including spectral information or gravitational lensing correction might improve these outer error bars.

version 2-1 to 2-2 after this plot was made, we refit SN SCP-0401 with the older SALT2-1 for the purposes of making this figure. The change in distance modulus is 0.01 magnitudes between the two versions.

The quality of these results at this extremely high redshift sets a new standard. Most SNe at $z > 1.5$ have incomplete or not cosmologically useful lightcurves (SN 1997ff from Riess et al. (2001), 2003ak from Riess et al. (2004), Subaru-Discovered SNe from Graur et al. (2011)). Primo (Rodney et al. 2012) has a lower-precision color measurement than SN SCP-0401, although its better x_1 measurement (by virtue of pre-maximum data) gives it a comparable distance modulus error. All of these previous SNe had no spectro-

scopic confirmation, or in the case of Primo, a host-contaminated spectrum providing inconclusive confirmation.

It has appeared likely that SNe at this redshift could be measured with sufficient color precision to allow a direct comparison to lower-redshift SNe. With this one SN, we now see a first example of this in Figure 6, a plot with a baseline of almost ten billion years (the approximate look back time of this SN). The Hubble residual of SN SCP-0401 is compatible with the x_1 and c corrections derived at lower redshift (or a deviation from Λ CDM of the Hubble diagram cancels the change in the relations). This figure also shows that the fitted x_1 and c of SN SCP-0401 are well within the distribution of lower-redshift

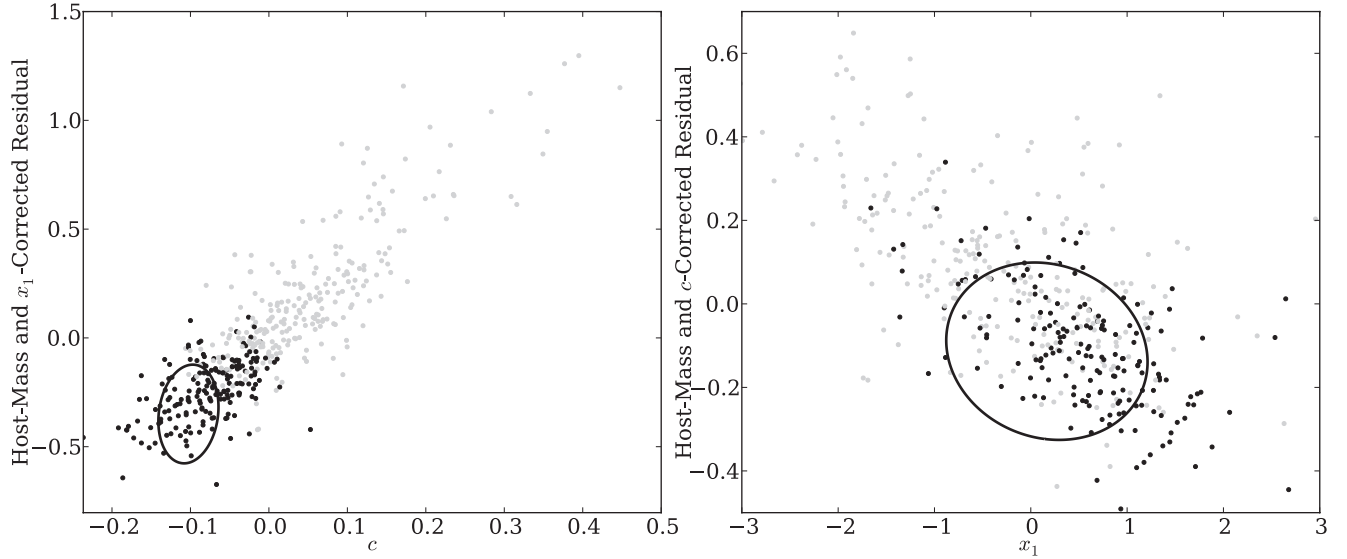


FIG. 6.— Plot of Hubble residuals (from the best-fit flat Λ CDM model) against c (left panel) and x_1 (right panel). In the left panel, the distance moduli have been corrected for x_1 and host mass, revealing the c -brightness relation. Similarly, the distance moduli in the right panel are corrected for c and host mass. Each ellipse represents the ($\Delta\chi^2 = 1$) SALT2-2 Gaussian approximation to the likelihood for SN SCP-0401; projecting the uncertainty to each axis gives the $1\text{-}\sigma$ error bars on each parameter. The points are comparison supernovae taken from Rubin et al. (in prep); for clarity, only SNe measured to better than 0.05 mag in c are shown. The black points represent SNe that would be bright enough in F850LP (at peak) to have been found at redshift 1.71 in our search.

supernovae that could be found in this F850LP search at redshift 1.71 (black points).

While the spectrum, light-curve corrections, and distance modulus of SN SCP-0401 so far indicate compatibility with Λ CDM and little evolution, this single SN by itself can only provide weak constraints. It does,

however, begin to illustrate what can be accomplished if one adds a whole population of such well-measured SNe at the very-high-redshift end of the Hubble diagram. Building this sample can now be done much more efficiently since the *HST* WFC3 greatly improved throughput makes these high S/N measurements easier, so this goal is now within reach.

APPENDIX

A. WEIGHT OF A SPECTRUM WITH NEAREST-NEIGHBOR CORRELATIONS

Suppose we have a spectrum with nearest-neighbor correlation ρ between wavelength elements. We can write the spectrum covariance matrix as

$$C = \sigma \cdot (I + A) \cdot \sigma \quad (\text{A1})$$

where $\sigma_{ij} = \sigma_i \delta_{ij}$, I is the identity matrix, and $A_{ij} = \rho[\delta(|i-j|-1)]$. We would like the total weight of the spectrum, the sum of C^{-1} . Writing

$$C^{-1} = \sigma^{-1} \cdot (I + A)^{-1} \cdot \sigma^{-1}, \quad (\text{A2})$$

we can focus on the $(I + A)^{-1}$ term. We begin by expanding this inverse as

$$(I + A)^{-1} = I + \sum_{k=1}^{\infty} (-1)^k A^k \quad (\text{A3})$$

We can now exchange the order of the matrix sum and series expansion and consider the sum of each term. The sum of I is N , while for very large matrices (so that we can ignore edge effects), the sum of A^k is $N(2\rho)^k$, which goes to zero if $|\rho| < 1/2$. The desired sum is then

$$\sum_{ij} (I + A)^{-1} = N \sum_{k=0}^{\infty} (-2\rho)^k = N/(1 + 2\rho) \quad (\text{A4})$$

for $|\rho| < 1/2$ as referenced in Section 3.1.

B. SPECTRAL PRINCIPAL COMPONENT ANALYSIS

As discussed in Section 3.3, we use a principal component analysis to allow comparisons between spectra with limited wavelength coverage and non-negligible noise, as well as to help establish the dimensionality of the parameter space, so that $\Delta\chi^2$ values can be converted into probabilities. We have opted to perform this principal component analysis in $\log(\text{flux})$ so that color variations can be more accurately modeled. As the signal-to-noise of most spectra is inadequate to simply take the log of the fluxes, we construct the principal components using an iterative fit.

We model each spectrum as

$$a_0 * c_0(\lambda) \exp[a_1 * c_1(\lambda) + a_2 * c_2(\lambda)] \quad (\text{B1})$$

where a_0 is the normalization, $c_0(\lambda)$ represents the mean, a_1 and a_2 are the projections onto the first and second components, and $c_1(\lambda)$ and $c_2(\lambda)$ are the first and second components.

We fit the mean and first component (0 and 1, above) and their projections first (with the second component fixed to zero). After convergence, we fit the mean and second component with the first component held fixed. This sequential procedure ensures that at every stage, the component we are fitting is the one that contributes the most variance remaining. We start versions of the fit with many randomly chosen initial values for the projections to ensure that we have a converged solution (the components are always initialized at zero). We exclude the models of [Lentz et al. \(2000\)](#) from training the components, but we do compute the projections to enable a quantitative comparison to SN SCP-0401.

We use an error floor to prevent extremely well-measured wavelength regions or spectra from dominating the analysis. The error floor required is that needed to obtain a χ^2 per degree of freedom of 1 for the residuals from the model. For our two-component analysis, this is S/N 5 per $\Delta\lambda/\lambda$ of 0.01 (a spectrum with $\Delta\lambda/\lambda$ of 0.001 would therefore be limited to S/N 1.6 per resolution element).

There is some ambiguity about how many principal components to use. Increasing the number allows for a smaller error floor (as more and more of the variance is described by the principal components). It also allows for better discrimination between spectra (e.g., spectra that are similar in the first two principal components may be dissimilar in the third). However, increasing the number also increases the $\Delta\chi^2$ values required for a given level of statistical significance. Two principal components are all that is necessary to fit almost all spectra to within the accuracy that the spectrum SN SCP-0401 has been measured; two are therefore used for the results of this paper.

As a test, we also compute the probability of SN SCP-0401 being a Ia (see Section 3.3) using one component and three components. Our results are robust; we find 93% confidence using one component, 92% confidence using two, and 91% confidence using three components. It is important to note that we chose to use two components before seeing any of these probabilities.

We would like to thank Henry Ferguson of the Space Telescope Science Institute for ensuring fast turnaround for these time-critical observations. We would also like to thank Bahram Mobasher for providing photometric redshifts for the host galaxies of our candidates. The archival WFC3 data used to obtain the host redshift were taken under HST GO Program 11600, PI Benjamin Weiner. We would like to thank the SUSPECT archive for their part in assembling our collection of spectra. Finally we thank the anonymous referee, whose feedback greatly improved this manuscript.

Financial support for this work was provided by NASA through program GO-9727 from the Space Telescope Science Institute, which is operated by AURA, Inc., under NASA contract NAS 5-26555. This work was also partially supported by the Director, Office of Science, Department of Energy, under grant DE-AC02-05CH11231.

Facilities: Hubble Space Telescope.

REFERENCES

- Aihara, H., Allende Prieto, C., An, D., et al. 2011, *ApJS*, 193, 29
 Amanullah, R., Lidman, C., Rubin, D., et al. 2010, *ApJ*, 716, 712
 Barbary, K., Aldering, G., Amanullah, R., et al. 2012, *ApJ*, 745, 31
 Bazin, G., Palanque-Delabrouille, N., Rich, J., et al. 2009, *A&A*, 499, 653
 Blanco, V. M., Schweizer, F., Moffat, A. F. J., et al. 1980, *IAU Circ.*, 3556, 2
 Bohlin, R. C. 2007, Photometric Calibration of the ACS CCD Cameras, Tech. rep.
 Branch, D., Lacy, C. H., McCall, M. L., et al. 1983, *ApJ*, 270, 123
 Branch, D., Benetti, S., Kasen, D., et al. 2002, *ApJ*, 566, 1005
 Brown, P. J. 2009, PhD thesis, The Pennsylvania State University
 Bufano, F., Immler, S., Turatto, M., et al. 2009, *ApJ*, 700, 1456
 Buta, R. J. 1982, *PASP*, 94, 578
 Buta, R. J., Corwin, Jr., H. G., & Opal, C. B. 1985, *PASP*, 97, 229
 Ciatti, F., Barbon, R., Cappellaro, E., & Rosino, L. 1988, *A&A*, 202, 15
 Clocchiatti, A., Phillips, M. M., Suntzeff, N. B., et al. 2000, *ApJ*, 529, 661
 Cowie, L. L., Barger, A. J., Hu, E. M., Capak, P., & Songaila, A. 2004, *AJ*, 127, 3137
 de Jong, R. S., Bergeron, E., Riess, A., & Bohlin, R. 2006, NICMOS count-rate dependent nonlinearity tests using flatfield lamps, Tech. rep.
 de Vaucouleurs, G., de Vaucouleurs, A., Buta, R., Ables, H. D., & Hewitt, A. V. 1981, *PASP*, 93, 36
 della Valle, M., Pasquini, L., Phillips, M., & McCarthy, P. 1990, *IAU Circ.*, 5079, 1
 Dickinson, M., Giavalisco, M., & GOODS Team. 2003, in *The Mass of Galaxies at Low and High Redshift*, ed. R. Bender & A. Renzini, 324
 Drescher, C., Parker, S., Brimacombe, J., Noguchi, T., & Nakano, S. 2011, *Central Bureau Electronic Telegrams*, 2940, 1
 Ellis, R. S., Sullivan, M., Nugent, P. E., et al. 2008, *ApJ*, 674, 51
 Evans, R. O., White, B., & Bembrick, C. 2001, *IAU Circ.*, 7772, 1
 Filippenko, A. V., Sargent, W. L. W., Kriss, G., et al. 1985, *IAU Circ.*, 4080, 1
 Filippenko, A. V., Matheson, T., Barth, A. J., et al. 1994, *IAU Circ.*, 5964, 1
 Foley, R. J., Smith, N., Ganeshalingam, M., et al. 2007, *ApJ*, 657, L105
 Foley, R. J., Papenkova, M. S., Swift, B. J., et al. 2003, *PASP*, 115, 1220
 Foley, R. J., Kromer, M., Howie Marion, G., et al. 2012, *ApJ*, 753, L5
 Fruchter, A. S., & Hook, R. N. 2002, *PASP*, 114, 144
 Ganeshalingam, M., Li, W. D., Chornock, R., & Filippenko, A. V. 2001, *IAU Circ.*, 7714, 4
 Garnavich, P. M., Kirshner, R. P., Challis, P., et al. 1998, *ApJ*, 493, L53
 Gibbons, R. A., Knop, R. A., Kuznetsova, N., & Supernova Cosmology Project Collaboration. 2004, in *Bulletin of the American Astronomical Society*, Vol. 36, American Astronomical Society Meeting Abstracts, 1460
 Gouiffes, C., Rosa, M., Melnick, J., et al. 1988, *A&A*, 198, L9
 Graur, O., Poznanski, D., Maoz, D., et al. 2011, *MNRAS*, 417, 916
 Guo, Q., White, S., Li, C., & Boylan-Kolchin, M. 2010, *MNRAS*, 404, 1111
 Guy, J., Sullivan, M., Conley, A., et al. 2010, *A&A*, 523, A7
 Hamuy, M., Phillips, M. M., Maza, J., et al. 1991a, *AJ*, 102, 208
 Hamuy, M., Phillips, M. M., Silva, D., Lubcke, G., & Steffey, P. 1991b, *IAU Circ.*, 5251, 1
 Hamuy, M., Pinto, P. A., Maza, J., et al. 2001, *ApJ*, 558, 615
 Herald, D., McNaught, R. H., Morel, M., et al. 1987, *IAU Circ.*, 4317, 1
 Hicken, M., Challis, P., Jha, S., et al. 2009, *ApJ*, 700, 331
 Holz, D. E., & Linder, E. V. 2005, *ApJ*, 631, 678
 Hopkins, A. M., & Beacom, J. F. 2006, *ApJ*, 651, 142
 Immler, S. 2005, in *Chandra Proposal*, 2292
 Jha, S., Challis, P., Garnavich, P., et al. 1999, *IAU Circ.*, 7296, 2
 Jönsson, J., Dahlén, T., Goobar, A., et al. 2006, *ApJ*, 639, 991
 Kawabata, K. S., Jeffery, D. J., Iye, M., et al. 2002, in *8th Asian-Pacific Regional Meeting, Volume II*, ed. S. Ikeuchi, J. Hearnshaw, & T. Hanawa, 333–334
 Kelly, P. L., Hicken, M., Burke, D. L., Mandel, K. S., & Kirshner, R. P. 2010, *ApJ*, 715, 743
 Kharadze, E. K., Pskovskiy, Y. P., Kimeridze, G. N., et al. 1989, *IAU Circ.*, 4802, 1
 Kimeridze, G. N., & Tsvetkov, D. Y. 1989, *Astrofizika*, 31, 17
 —. 1991, *Soviet Ast.*, 35, 168
 Kirshner, R., & Bryan, J. 1980, *IAU Circ.*, 3534, 2
 Kirshner, R., Blondin, S., Chevalier, R., et al. 2010, *The Astronomer's Telegram*, 2513, 1
 Knop, R. A., Aldering, G., Amanullah, R., et al. 2003, *ApJ*, 598, 102
 Koekemoer, A. M., Fruchter, A. S., Hook, R. N., & Hack, W. 2002, in *The 2002 HST Calibration Workshop : Hubble after the Installation of the ACS and the NICMOS Cooling System*, ed. S. Arribas, A. Koekemoer, & B. Whitmore, 337
 Korth, S. 1989, *BAV Rundbrief*, 38, 88
 Kowalski, M., Rubin, D., Aldering, G., et al. 2008, *ApJ*, 686, 749
 Kümmel, M., Walsh, J. R., Pirzkal, N., Kuntschner, H., & Pasquali, A. 2009, *PASP*, 121, 59
 Le Borgne, D., & Rocca-Volmerange, B. 2002, *A&A*, 386, 446
 Leibundgut, B., Kirshner, R. P., Filippenko, A. V., et al. 1991, *ApJ*, 371, L23
 Lentz, E. J., Baron, E., Branch, D., Hauschildt, P. H., & Nugent, P. E. 2000, *ApJ*, 530, 966
 Li, W., Leaman, J., Chornock, R., et al. 2011, *MNRAS*, 412, 1441
 Li, W.-D., Li, C., Filippenko, A. V., & Moran, E. C. 1998, *IAU Circ.*, 6829, 1
 Liller, W., Brown, N., McNaught, R. H., et al. 1992, *IAU Circ.*, 5428, 1
 Liu, Q.-Z., Hu, J.-Y., Hang, H.-R., et al. 2000, *A&AS*, 144, 219
 Matheson, T., Jha, S., Challis, P., Kirshner, R., & Huchra, J. 2001, *IAU Circ.*, 7731, 3
 Mattei, J., Johnson, G. E., Rosino, L., Rafanelli, P., & Kirshner, R. 1979, *IAU Circ.*, 3348, 1
 Maury, A., Thouvenot, E., Buil, C., et al. 1990, *IAU Circ.*, 5039, 1
 Modjaz, M., Kirshner, R., Challis, P., & Berlind, P. 2005a, *Central Bureau Electronic Telegrams*, 160, 1
 Modjaz, M., Kirshner, R., Challis, P., & Hutchins, R. 2005b, *Central Bureau Electronic Telegrams*, 174, 1
 Navarro, J. F., Frenk, C. S., & White, S. D. M. 1996, *ApJ*, 462, 563
 Nomoto, K., Thielemann, F.-K., & Yokoi, K. 1984, *ApJ*, 286, 644
 Panagia, N. 1985, in *Lecture Notes in Physics*, Berlin Springer Verlag, Vol. 224, *Supernovae as Distance Indicators*, ed. N. Bartel, 14–33
 Panagia, N. 2003, in *Lecture Notes in Physics*, Berlin Springer Verlag, Vol. 598, *Supernovae and Gamma-Ray Bursters*, ed. K. Weiler, 113–144
 Pastorello, A., Valenti, S., Zampieri, L., et al. 2009, *MNRAS*, 394, 2266
 Perlmutter, S., Aldering, G., della Valle, M., et al. 1998, *Nature*, 391, 51
 Perlmutter, S., Aldering, G., Goldhaber, G., et al. 1999, *ApJ*, 517, 565
 Phillips, M. M., Suntzeff, N. B., Krisciunas, K., et al. 2001, *IAU Circ.*, 7772, 2
 Phillips, M. M., Wells, L. A., Suntzeff, N. B., et al. 1992, *AJ*, 103, 1632
 Polcaro, V. F., & Viotti, R. 1991, *A&A*, 242, L9
 Prabhu, T. P. 1985, *Bulletin of the Astronomical Society of India*, 13, 68
 —. 1995, *Journal of Astrophysics and Astronomy Supplement*, 16, 317
 Prabhu, T. P., & Krishnamurthi, A. 1990, *A&A*, 232, 75
 Riess, A. G., Filippenko, A. V., Challis, P., et al. 1998, *AJ*, 116, 1009
 Riess, A. G., Nugent, P. E., Gilliland, R. L., et al. 2001, *ApJ*, 560, 49

- Riess, A. G., Strolger, L.-G., Tonry, J., et al. 2004, *ApJ*, 607, 665
Riess, A. G., Strolger, L.-G., Casertano, S., et al. 2007, *ApJ*, 659, 98
Ripoche, P., Aldering, G., Amanullah, R., et al. *ApJ* Submitted
Rodney, S. A., Riess, A. G., Dahlen, T., et al. 2012, *ApJ*, 746, 5
Sasaki, M., Kosugi, G., Ishigaki, T., et al. 1994, *PASJ*, 46, L187
Sonneborn, G., Kirshner, R., della Valle, M., et al. 1990, *IAU Circ.*, 5034, 1
Stringfellow, G. S., Howell, S. B., Probst, R., & Seebode, S. 2011, *The Astronomer's Telegram*, 3428, 1
Sullivan, M., Conley, A., Howell, D. A., et al. 2010, *MNRAS*, 406, 782
Suntzeff, N., Parker, J., Hunter, D., et al. 1992, *IAU Circ.*, 5432, 2
Suzuki, N., Rubin, D., Lidman, C., et al. 2012, *ApJ*, 746, 85
Szeidl, B., Lovas, M., Barbon, R., et al. 1982, *IAU Circ.*, 3671, 1
Tsvetkov, D. Y., Volkov, I. M., Sorokina, E., et al. 2012, *Peremennye Zvezdy*, 32, 6
Uomoto, A., & Kirshner, R. P. 1985, *A&A*, 149, L7
Vettolani, G., Marano, B., Zitelli, V., et al. 1981, *IAU Circ.*, 3584, 1
Wamsteker, W., Talavera, A., Machetto, F., et al. 1983, *IAU Circ.*, 3791, 2
Wang, Y., Holz, D. E., & Munshi, D. 2002, *ApJ*, 572, L15
Ward, M. J., Blades, J. C., & Griffiths, R. E. 1978, *IAU Circ.*, 3309, 1
Wheeler, J. C., & Levreault, R. 1985, *ApJ*, 294, L17